Journal of Pathology
J Pathol July 2022; **257:** 352–366
Published online 13 April 2022 in Wiley Online Library
(wileyonlinelibrary.com) **DOI:** 10.1002/path.5895

ORIGINAL ARTICLE

Selective ablation of Nfix in macrophages attenuates muscular dystrophy by inhibiting fibro–adipogenic progenitor–dependent fibrosis

Marielle Saclier[1†], Giuseppe Angelini[1], Chiara Bonfanti[1], Giada Mura[1], Giulia Temponi[1] and Graziella Messina[1*]

[1] *Department of Biosciences, University of Milan, Milan, Italy*

**Correspondence to: G Messina, Department of Biosciences, University of Milan, via Celoria 26, 20133 Milan, Italy. E-mail: graziella.messina@unimi.it*

[†]*Present address:* Cellular Plasticity and Disease Modeling, Department of Developmental and Stem Cell Biology, CNRS UMR 3738, Institut Pasteur, Paris, France

Abstract

Muscular dystrophies are genetic diseases characterized by chronic inflammation and fibrosis. Macrophages are immune cells that sustain muscle regeneration upon acute injury but seem deleterious in the context of chronic muscle injury such as in muscular dystrophies. Here, we observed that the number of macrophages expressing the transcription factor Nfix increases in two distinct mouse models of muscular dystrophies. We showed that the deletion of Nfix in macrophages in dystrophic mice delays the establishment of fibrosis and muscle wasting, and increases grasp force. Macrophages lacking Nfix expressed more TNFα and less TGFβ1, thus promoting apoptosis of fibro–adipogenic progenitors. Moreover, pharmacological treatment of dystrophic mice with a ROCK inhibitor accelerated fibrosis through the increase of Nfix expression by macrophages. Thus, we have identified Nfix as a macrophage profibrotic factor in muscular dystrophies, whose inhibition could be a therapeutic route to reduce severity of the dystrophic disease.

Keywords: macrophage; Nfix; muscular dystrophy; fibrosis; inflammation; fibro-adipogenic progenitors

Received 9 September 2021; Revised 24 February 2022; Accepted 15 March 2022

No conflicts of interest were declared.

Introduction

Muscular dystrophies (MDs) are a heterogeneous group of inherited disorders caused by mutations in genes coding for components of the structural dystrophin–glycoprotein complex that induce its disassembly. This leads to sarcolemma fragility and myofiber necrosis especially during intense contractile activity, provoking cycles of regeneration–degeneration [1–3]. These continuous cycles induce muscle wasting, chronic inflammation, and fibrosis, which can cause patients' death [4,5]. MDs remain incurable and currently, drug therapy brings only limited results. Chronic use of glucocorticoids delays the progression of MDs but has numerous side effects such as bone fragility, weight gain, and muscle weakness [6–9].

Dystrophic muscle cells are at the origin of the disease, but several other cell types participate in MD progression. While the timely appearance of specific populations of macrophages (MPs) is required for successful muscle regeneration upon acute injury, it is not clear if MPs act negatively or positively in MDs. General impediment of MP infiltration within the *mdx* muscle, a mouse model for Duchenne muscular dystrophy (DMD), improves both muscle histology and function [10–12]. However, a recent study demonstrated that a decrease of MP infiltration induced by blood monocyte depletion promotes the conversion of satellite cells (SCs), the muscle stem cells, into adipocytes [13]. Anti-inflammatory TGFβ1, which is secreted mainly by MPs, induces the expression of extracellular matrix (ECM) components by fibro-adipogenic progenitors (FAPs) and thus promotes fibrosis [14–16], but, conversely, pro-inflammatory markers have been associated with the profibrotic function of MPs and DMD worsening [17–20]. More than simply the presence or absence of MPs, their phenotype and secretion of specific cytokines seem to have an important function in MD progression.

Nuclear factor I X (Nfix) is a transcription factor belonging to the highly conserved DNA-binding nuclear factor I family [21]. We demonstrated previously the essential function of Nfix expression by myogenic cells during muscle development [22] and regeneration upon acute injury [23]. Importantly, the total deletion of Nfix in two murine models of MDs improves muscle histology and function [24]. Nfix is also important for the

correct phenotypic switch and function of MPs upon acute muscle injury. In particular, ROCK inhibition stimulates phagocytosis in MPs, which induces the expression of Nfix that drives a decrease of pro-inflammatory markers and an increase of anti-inflammatory markers [25].

Here, we demonstrated that Nfix expression by MPs during development of dystrophy is associated with its progression by acting both on myogenic cells and FAPs. *Nfix*-specific deletion in α-sarcoglycan null mice (hereafter called *Sgca* null), the mouse model for limb–girdle muscular dystrophy 2D, protects myofibers from apoptosis and decreases the establishment of fibrosis, leading to increased grasp force. We showed that MPs with *Nfix* deleted express more TNFα and less TGFβ1, inducing apoptosis of FAPs. Moreover, pharmacological inhibition of ROCK in *Sgca* null mice accelerated fibrosis by increasing the number of MPs expressing Nfix. With this study, we have demonstrated that Nfix expression by MPs is involved in the progression of MDs *in vivo*. Targeting Nfix in MPs could represent a valid approach to delay muscle wasting and fibrosis in MDs.

Materials and methods

Animal models and *in vivo* experimentation

Mdx, *Sgca* null, $Nfix^{fl/fl}$:$\alpha^{(-/-)}$ (for $Nfix^{fl/fl}$:$sgca^{(-/-)}$), $\Phi Nfix^{(-/-)}$:$\alpha^{(+/-)}$ (for $LysM^{CRE}$:$Nfix^{fl/fl}$:$sgca^{(+/-)}$), and $\Phi Nfix^{(-/-)}$:$\alpha^{(-/-)}$ (for $LysM^{CRE}$:$Nfix^{fl/fl}$:$sgca^{(-/-)}$) mice were used in this study. $\Phi Nfix^{(-/-)}$:$\alpha^{(-/-)}$ (for $LysM^{CRE}$:$Nfix^{fl/fl}$:$sgca^{(-/-)}$) mice were generated by crossing $\Phi Nfix^{(-/-)}$ (or $LysM^{CRE}$:$Nfix^{fl/fl}$) mice with the *Sgca* null mice [25,26]. The $LysM^{CRE}$ mouse is used to abbreviate B6.129P2-Lyz2tm1(cre)Ifo/J mouse. All mice having the $LysM^{CRE}$ gene were heterozygous for it. For some experiments, 10-week-old *Sgca* null mice and $\Phi Nfix^{(-/-)}$:$\alpha^{(-/-)}$ (for $LysM^{CRE}$:$Nfix^{fl/fl}$:$sgca^{(-/-)}$) mice were injected i.p. with saline solution or Y-27632 ROCK1 inhibitor (10 mg/kg, sc-281642; Santa Cruz Biotechnology, Dallas, TX, USA) 3 times per week for 2 weeks. Mice were kept in pathogen-free conditions, and all procedures conformed to Italian law (D. Lgs n° 2014/26, implementation of the 2010/63/UE) and were approved by the University of Milan Animal Welfare Body and by the Italian Minister of Health.

Histology and immunofluorescence analyses

The fascia of tibialis anterior (TA) muscles was removed, and muscles were frozen in liquid nitrogen-cooled isopentane (VWR, Radnor, PA, USA) and stored at −80 °C until cut. Eight-micrometer-thick cryosections were stained using hematoxylin and eosin (H&E) or Milligan's trichrome, or were used for immunofluorescence. For some experiments, the weights of TA muscles and mice were recorded.

H&E staining was processed according to standard protocols. For Milligan's trichrome staining, sections were fixed for 1 h with Bouin's fixative (Sigma-Aldrich, Burlington, MA, USA) and rinsed for 1 h under running water. Sections were then dehydrated to 95% EtOH in graded ethanol solutions, successively passed in 3% potassium dichromate (Sigma-Aldrich) for 5 min, washed in distilled water, stained with 0.1% acid fuchsin (Sigma-Aldrich) for 30 s, washed again in distilled water, passed in 1% phosphomolybdic acid (Sigma-Aldrich) for 3 min, stained with Orange G (2% in 1% phosphomolybdic acid; Sigma-Aldrich) for 5 min, rinsed in distilled water, passed in 1% acetic acid (VWR) for 2 min, stained with 1% Fast Green for 5 min (Sigma-Aldrich), placed in 1% acetic acid for 3 min, rapidly dehydrated to 100% EtOH, and placed in xylene before mounting with Eukitt (Bio-Optica, Milano, Italy).

For immunofluorescence analysis, sections or cells were fixed for 15 min with 4% paraformaldehyde (except for F4/80). Then samples were permeabilized with 0.5% Triton X-100 (Sigma-Aldrich) in PBS for 10 min and blocked with 4% BSA (Sigma-Aldrich) in PBS at room temperature for 1 h. Primary antibodies were incubated overnight at 4 °C in PBS. After three washes of 5 min with PBS, samples were incubated with secondary antibodies (1:500; Jackson ImmunoResearch, Cambridge, UK; fluorochromes used: 488 and 594) and Hoechst (1:500, Sigma-Aldrich) in PBS for 45 min at room temperature, then washed 4 times for 5 min with PBS and mounted with Fluorescence Mounting Medium (Sigma-Aldrich). For Nfix-F4/80 double immunolabeling, cryosections were labeled with antibodies against F4/80 (1:400, NB300-605; Novus Biologicals, Centennial, CO, USA) overnight at 4 °C, and Nfix labeling using NBP2-15038 antibody (1:200, Novus Biologicals) was performed for 2 h at 37 °C. Pax7 immunolabeling was done on fresh cut muscle sections and antigen retrieval was performed by incubating muscle sections in boiling 10 mM citrate buffer, pH 6 for 20 min. Muscle sections were then incubated overnight with Pax7 (1:2; Developmental Studies Hybridoma Bank, Iowa City, IA, USA). Anti-collagen I (1:200, 1310-01; Southern Biotech, Birmingham, AL, USA), anti-PDGFRα (1/500, AF1062; R&D Systems, Minneapolis, MN, USA), and anti-laminin (1:300, L9393, Sigma-Aldrich) antibodies were used on muscle sections. Anti-TNFα (1:100, GTX54419; Genetex, Irvine, CA, USA), anti-TGFβ1 (1:100, ab64715; Abcam, Cambridge, UK), anti-cleaved caspase-3 (1:300, 9661S; Cell Signaling Technology, Danvers, MA, USA), and anti-Ki67 (1:50, 550609; BD Biosciences, Franklin Lakes, NJ, USA) antibodies were used on FAPs or sorted MP cells.

Evans blue dye uptake

Evans blue dye (solution at 5 mg/ml, Sigma-Aldrich) was injected 24 h intraperitoneally before sacrifice (10 µl per g of mouse). Positivity for Evans blue dye was revealed through its fluorescence after excitation at 546 nm. Sections were fixed with acetone (VWR) for 10 min at −20 °C, permeabilized in 0.5% Triton X-100 (Sigma-Aldrich) for 10 min, blocked for 1 h in 4% BSA, and incubated overnight with rabbit anti-

laminin antibody (1:300, Sigma-Aldrich) to reveal myofiber outlines. The day after, sections were washed, incubated with a goat anti-rabbit 488 secondary antibody (1:250, Jackson ImmunoResearch) and Hoechst (1:500, Sigma-Aldrich) in PBS for 45 min at room temperature, then washed 4 times for 5 min with PBS and mounted with Fluorescence Mounting Medium (Sigma-Aldrich). Measurement of the percentage of Evans blue dye uptake was performed by counting the number of Evans blue dye-positive fibers on total muscle section reconstructions, using ImageJ software (NIH, Bethesda, MD, USA).

RNA extraction and RT-qPCR

RNA was isolated from TA using TRIzol Reagent (15596026, Invitrogen) according to the manufacturer's instructions. RNA was quantified using a NanoPhotometer (Implen, München, Germany). For reverse transcription, 500 ng of RNA was used with an iScript Reverse Transcription Supermix for RT-quantitative qPCR (1708840; Bio-Rad, Hercules, CA, USA). For qPCR, cDNA was diluted 1:10 and 5 µl of the diluted cDNA was loaded in a total volume of 20 µl of SYBR Green Supermix (172-5124, Bio-Rad) and run on a Bio-Rad CFX Connect Real-Time PCR System. The relative quantification of gene expression was determined by the comparative CT method and normalized to *Gapdh*. The following primers were used: Tgfb1 forward AACAACGCCATCTATGAGAAAACC; Tgfb1 reverse CCGAATGTCTGACGTATTGAAGAA; fibronectin (*Fn1*) forward AGGACTGGCATTCACTGATGTG; fibronectin (*Fn1*) reverse GTCACCCTGTACCTGGAAACTTG; αSMA (*Acta2*) forward GTACCACCATGTACCCAGGC; αSMA (*Acta2*) reverse: GCTGGAAGGTAGACAGCGAA; *Gapdh* forward AGGTCGGTGTGAACGGATTTG; *Gapdh* reverse TGTAGACCATGTA GTTGAGGTCA.

Protein extraction and immunoblotting

Protein extracts were obtained from TA lysed using RIPA buffer [10 mM Tris–HCl (pH 8.0), 1 mM EDTA, 1% Triton X-100, 0.1% sodium deoxycholate, 0.1% sodium dodecylsulfate (SDS), 150 mM NaCl, in deionized water] plus protease and phosphatase inhibitors for 30 min on ice. Then, samples were centrifuged at 11 000 × *g* for 10 min at 4 °C, and the supernatants collected for protein quantification (DC Protein Assays, 5000111, Bio-Rad). Aliquots (40 µg protein) of each sample were denatured at 95 °C for 5 min in SDS PAGE sample-loading buffer [100 mM Tris (pH 6.8), 4% SDS, 0.2% bromophenol blue, 20% glycerol, 10 mM dithiothreitol] and loaded onto 8% SDS acrylamide gels. After electrophoresis, the protein was blotted onto nitrocellulose membranes (Whatman Protran nitrocellulose transfer membrane, Sigma-Aldrich) for 2 h at 70 V, 4 °C. Membranes were then blocked for 1 h with 5% dried milk powder in Tris-buffered saline plus 0.02% Tween 20 (Sigma-Aldrich). Membranes were incubated with primary antibodies overnight at 4 °C, using the following antibodies: rabbit anti-P-Smad3 (1:2000, ab52903, Abcam), rabbit anti-Tot-Smad3 (1:1000, #9523, Cell Signaling Technology), and mouse anti-vinculin (1:2500, V9131, Sigma-Aldrich). After incubation with the primary antibodies, the membranes were washed 3 times for 5 min and incubated with a secondary antibody (1:10 000, IgG-HRP, Bio-Rad) for 45 min at room temperature, and then washed again 5 times for 5 min. Bands were revealed using ECL detection reagent (Thermo Fisher Scientific, Waltham, MA, USA), with images acquired using a ChemiDoc MP system (Bio-Rad). After incubation with rabbit anti-P-Smad3 antibody, the 4-month TA sample membrane was stripped with a mild stripping solution (200 mM glycine, 1% SDS, 10% Tween 20, pH 2.2). After verification of stripping by incubating membrane with anti-rabbit-HRP secondary antibody for 45 min at room temperature, the membrane was then incubated with anti-Tot-Smad3 antibody overnight. Image Lab software (Bio-Rad) was used to measure and quantify the bands of at least three independent samples. The obtained absolute quantity was compared with the reference band (vinculin) and expressed in the graphs as normalized volume (Norm. Vol. Int.).

Isolation of MPs and FAPs from skeletal muscle

The fascia of TA muscles was removed; then muscles were dissociated and digested in RPMI medium containing 0.2% (w/v) collagenase B (11088815001; Roche Diagnostics GmbH, Mannheim, Germany) at 37 °C for 1 h and passed through a 70 µm and then a 30 µm cell strainer (Miltenyi Biotec, Bergisch Gladbach, Germany). $CD45^+$ cells were isolated using magnetic beads (130-052-301, Miltenyi Biotec) and incubated with FcR blocking reagent (130-059-901, Miltenyi Biotec) for 20 min at 4 °C in PBS with 2% FBS. $CD45^+$ cells were then incubated with Ly6C-PE (12-5932; eBioscience, San Diego, CA, USA) and CD64-APC (558539, BD Biosciences) antibodies for 30 min at 4 °C. $CD45^-$ cells were incubated with CD31-FITC (1:1000, 11-0311-82; Invitrogen, Waltham, MA, USA), CD45-FITC (1:1000, 11-0451-82, Invitrogen), ITAG7(a7)-APC (1:1000, MA5-23555, Invitrogen), and Sca1-PeCy7 (1:5000, 25-5981-82, Invitrogen) antibodies for 30 min at 4 °C. MPs ($CD64^+$ cells) and FAPs ($CD31^-/CD45^-/a7^-/Sca1^+$ cells) were analyzed and sorted using a FACS Aria III Cell Sorter (BD Biosciences) with a purity of 96.9% and 97.5%, respectively. In some experiments, $Ly6C^+$ and $Ly6C^-$ MPs, or $CD64^+$ MPs and FAPs were cytospinned on StarFrost (Knittel, Braunschweig, Germany) slides and immunostained.

Treadmill test and grasp strength test

For the treadmill test functional assay, 4-week-old mice were exercised 3 times, once a week, before recording their performances. The treadmill test was therefore performed starting from 7-week-old mice, once a week for 6 weeks. The test was conducted on a treadmill (Bioseb, Vitrolles, France) with a 10% incline, starting

from a speed of 6 cm/s and increasing it by 2 cm/s every 2 min. For each test, the time to exhaustion of each mouse was measured.

For the grasp strength test functional assay, 2- and 6-month-old mice were tested 3–5 times by using a grid connected to a dynamometer. The average force in millinewtons (mN) was graphed as a measure of grasp strength.

Image acquisition and assessment

Images were acquired using an inverted microscope (Leica DMI6000 B; Leica Microsystems, Wetzlar, Germany) equipped with Leica DFC365FX and DFC400cameras and 10×, 20×, and 40× magnification objectives. For each condition of each experiment, at least eight fields chosen randomly were assessed. Measurement of central nucleation and myofiber cross-sectional area (CSA) was performed using ImageJ software. At least 500 myofibers per mouse were analyzed. Collagen I quantification was performed using a macro in ImageJ to identify and quantify positive areas. The number of labeled MPs or FAPs was calculated using the cell tracker in ImageJ software and expressed as a percentage of total MPs or FAPs.

Statistical analyses

All data shown in plots are expressed as mean ± SEM. All experiments were performed using at least three different animals in independent experiments. Statistical analysis was performed using two-tailed unpaired Student's *t*-tests, one-way ANOVA or two-way ANOVA (*$p < 0.05$; **$p < 0.01$; ***$p < 0.001$; $^{\$}p < 0.05$; $^{\$\$}p < 0.01$; $^{\$\$\$}p < 0.001$; confidence intervals 95%; α level 0.05).

Results

Nfix-positive MPs increase with the progression of muscular dystrophy

MPs are linked to MDs [17,20,27,28] and as we demonstrated a pivotal function of Nfix in MP function during muscle regeneration [25], we decided to analyze the number of Nfix$^+$ MPs during the progression of MD within the tibialis anterior (TA) and diaphragm (Dia) of the *mdx* and *Sgca* null dystrophic mouse models. We observed an increased number of MPs expressing Nfix in muscles of both *mdx* and *Sgca* null mice from 2 to 6 months (Figure 1A,B and supplementary material, Figure S1A,B). During muscle regeneration after acute injury, we showed that Nfix is required for Ly6C$^-$ anti-inflammatory phenotype acquisition [25]. Although the concept of pro- and anti-inflammatory MPs does not seem to be conserved in the context of chronic muscle injury compared to acute muscle injury, we decided to look at the number CD64$^+$ MPs positive for Nfix within the Ly6C$^+$ and Ly6C$^-$ populations sorted from the TA of *Sgca* null mice. In contrast to what happens during acute damage, Nfix was found at comparable levels between Ly6C$^+$/CD64$^+$ and Ly6C$^-$/CD64$^+$ MPs, and its expression increased by the same extent from 2 to 4 months in both populations in dystrophic muscles (Figure 1C). These results suggest an involvement of Nfix in MPs in MD progression and confirm the current knowledge that Ly6C$^+$ and Ly6C$^-$ MPs have different biological functions depending on whether the context is acute or chronic muscle injury.

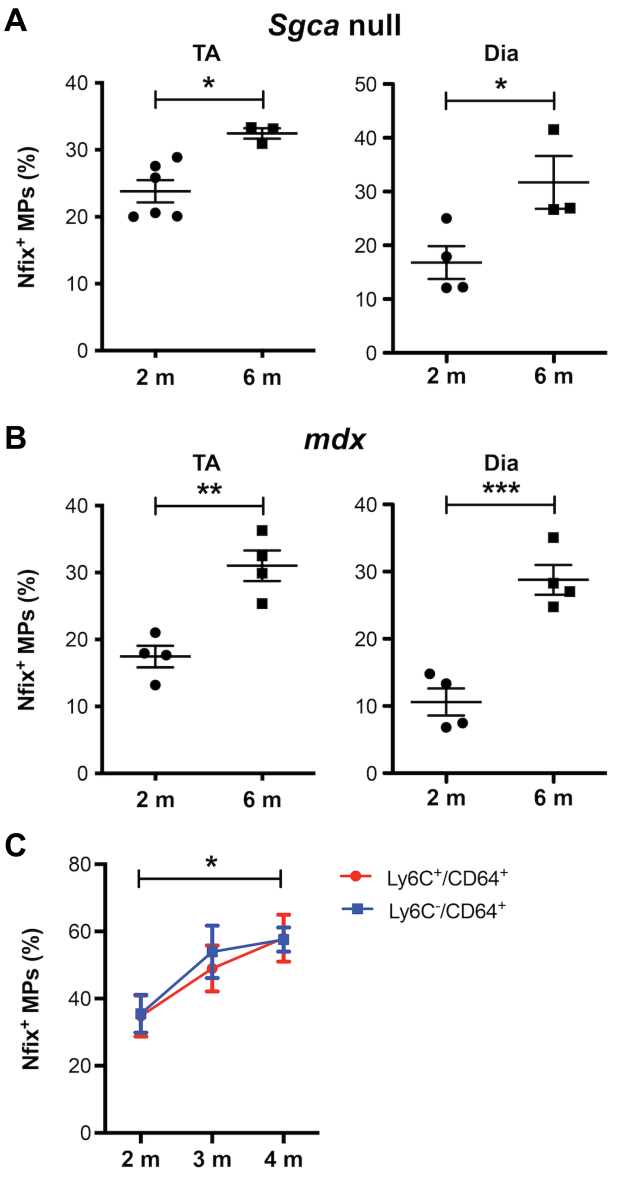

Figure 1. The number of Nfix$^+$ MPs increases with age in *Sgca* null and *mdx* mice. (A, B) Percentage of F4/80$^+$ MPs positive for Nfix in tibialis anterior muscles (TA) and diaphragm (Dia) of *Sgca* null mice (A) and *mdx* mice (B) at 2 and 6 months of age. (C) Percentage of Ly6C$^+$/CD64$^+$ and Ly6C$^-$/CD64$^+$ sorted MPs positive for Nfix from the TA of *Sgca* null mice at 2, 3, and 4 months of age. Statistical significance was determined using a two-tailed Student's *t*-test, one-way ANOVA test or two-way ANOVA test. *$p < 0.05$, **$p < 0.01$, ***$p < 0.001$. For C, *$p < 0.05$ Ly6C$^-$ 2 months versus 4 months. Means ± SEM. $N = 3$–6 mice per group.

Ablation of Nfix in MPs protects the dystrophic muscle

We previously demonstrated that Nfix silencing delays the progression of MD [24]. To understand to what

extent the rescue of dystrophic phenotype was due to the lack of Nfix in MPs, we generated *Sgca* null dystrophic mice in which Nfix is deleted in MPs: the LysM^{CRE}:Nfix$^{fl/fl}$:sgca$^{(-/-)}$ mice (hereafter named ΦNfix$^{(-/-)}$:α$^{(-/-)}$). We used the *Sgca* null mouse model because its phenotype better recapitulates the progression of DMD patients than *mdx* mice [4,26,29,30]. LysM^{CRE}:Nfix$^{fl/fl}$:sgca$^{(+/-)}$ (hereafter named ΦNfix$^{(-/-)}$:α$^{(+/-)}$) mice and Nfix$^{fl/fl}$:sgca$^{(-/-)}$ (hereafter named Nfix$^{fl/fl}$:α$^{(-/-)}$) mice were used as non-dystrophic and dystrophic controls, respectively. We looked at TA histology at 2, 4, and 6 months by H&E staining (Figure 2A and supplementary material, Figure S2A). Consistent with our previous observation in ΦNfix$^{(-/-)}$ mice [25], non-dystrophic ΦNfix$^{(-/-)}$:α$^{(+/-)}$ mice displayed a homogeneous caliber of myofibers with myonuclei in peripherical positions (Figure 2A and supplementary material, Figure S2A). Conversely, the muscle structure of the dystrophic control Nfix$^{fl/fl}$:α$^{(-/-)}$ mice at 2 months was characterized by necrotic myofibers, centrally nucleated myofibers, and inflammation. At 4 months, small and large fibers were present in the same muscles. All these features worsened at 6 months (Figure 2A and supplementary material, Figure S2A). In the ΦNfix$^{(-/-)}$:α$^{(-/-)}$ TA, myofibers in regeneration with few inflammatory areas, were detected (Figure 2A and supplementary material, Figure S2A). The CSA distribution of the non-dystrophic control exhibited a bell shape characteristic of WT muscles (Figure 2B). At 2 months, the CSA distribution was identical for the Nfix$^{fl/fl}$:α$^{(-/-)}$ and ΦNfix$^{(-/-)}$:α$^{(-/-)}$ mice. Over time, a shift towards an increase of small myofibers was observed in the Nfix$^{fl/fl}$:α$^{(-/-)}$ mice, while the CSA distribution of ΦNfix$^{(-/-)}$:α$^{(-/-)}$ mice remained unmodified up to 6 months (Figure 2B). We then analyzed the number of regenerative myofibers by quantifying the percentage of centrally nucleated myofibers. Almost no regenerating myofibers were detected in the ΦNfix$^{(-/-)}$:α$^{(+/-)}$ mice. In the Nfix$^{fl/fl}$:α$^{(-/-)}$ mice, 86% of myofibers were regenerative at 2 months and reached 92% at 6 months (supplementary material, Figure S3A). A significant decrease of the percentage of regenerative myofibers was observed in the ΦNfix$^{(-/-)}$:α$^{(-/-)}$ mice compared with the Nfix$^{fl/fl}$:α$^{(-/-)}$ mice at 2 months, which disappeared at 4 and 6 months (supplementary material, Figure S3A). We then analyzed an important hallmark of dystrophies, that is, myofiber fragility, using Evans blue (EB). As expected, we did not detect EB^{+} myofibers in the TA of ΦNfix$^{(-/-)}$:α$^{(+/-)}$ mice (Figure 2C,D). In the Nfix$^{fl/fl}$:α$^{(-/-)}$ mice, we observed that damaged myofibers appeared in foci and the quantification revealed a huge heterogeneity in the percentage of necrotic myofibers between animals. At 6 months, few EB^{+} myofibers were present, except for one TA reaching 35% of damaged myofibers (Figure 2D). On the contrary, the percentage of necrotic myofibers in the TA of ΦNfix$^{(-/-)}$:α$^{(-/-)}$ mice was homogeneous and strikingly low (Figure 2C,D). All these results demonstrate that Nfix deletion in MPs has a positive effect on the fragility of myofibers, delaying the appearance of regenerating myofibers and protecting dystrophic muscle.

Fibrosis decreases in the absence of Nfix in MPs

In time, dystrophic muscle is replaced by fibrotic tissue that can be highlighted in blue after Milligan trichrome staining. The ECM appeared thin between the myofibers in the TA of ΦNfix$^{(-/-)}$:α$^{(+/-)}$ mice (Figure 3A and supplementary material, Figure S2B). At 2 months, the TA of Nfix$^{fl/fl}$:α$^{(-/-)}$ mice presented large deposits of ECM which increased until 6 months (Figure 3A and supplementary material, Figure S2B). On the contrary, the TA of ΦNfix$^{(-/-)}$:α$^{(-/-)}$ mice exhibited less ECM than the Nfix$^{fl/fl}$:α$^{(-/-)}$ mice, with no large areas observed (Figure 3A and supplementary material, Figure S2B). We then performed immunofluorescence staining for collagen I and we quantified the positive area. Around 5% of collagen I was present in the TA of ΦNfix$^{(-/-)}$:α$^{(+/-)}$ mice, and Nfix$^{fl/fl}$:α$^{(-/-)}$ mice contained more than 20% of collagen I at all time points (Figure 3B,C). The TA of ΦNfix$^{(-/-)}$:α$^{(-/-)}$ mice displayed a significant reduction of collagen I deposits compared with Nfix$^{fl/fl}$:α$^{(-/-)}$ mice (Figure 3C). All these histological differences, however, did not induce a modification of the TA muscle mass (supplementary material, Figure S3B). To understand if the improvement of dystrophic muscle histology might also correlate with better muscle functionality, we carried out a treadmill and grasp strength test. For the treadmill test, no differences in the total and weekly running times between Nfix$^{fl/fl}$:α$^{(-/-)}$ and ΦNfix$^{(-/-)}$:α$^{(-/-)}$ mice were observed (supplementary material, Figure S3C). On the contrary, Nfix$^{fl/fl}$:α$^{(-/-)}$ mice had a reduced grasp force compared with ΦNfix$^{(-/-)}$:α$^{(+/-)}$ mice, while no difference was observed compared with ΦNfix$^{(-/-)}$:α$^{(-/-)}$ mice at 2 months (supplementary material, Figure S3D). At 6 months, no differences in grasp force were observed between any of the genotypes (supplementary material, Figure S3D). These results demonstrate that the lack of Nfix in MPs improves several dystrophic signs of the disease, inducing an increase of muscle grasp strength during early life. On the contrary, no muscle performance was observed when mice were forced to run, which likely depends on muscle cells.

Ablation of Nfix in MPs preserves the diaphragm from fibrosis

We also analyzed diaphragmatic histology because it better reflects the dystrophic phenotype [29,31]. Normal histology was observed in ΦNfix$^{(-/-)}$:α$^{(+/-)}$ mice, while the diaphragm (Dia) of Nfix$^{fl/fl}$:α$^{(-/-)}$ mice exhibited a worsened phenotype than the TA; conversely, the Dia of ΦNfix$^{(-/-)}$:α$^{(-/-)}$ mice displayed a better histology compared with the dystrophic control (Figure 4A and supplementary material, Figure S4A). After Milligan trichrome staining, we observed that ΦNfix$^{(-/-)}$:α$^{(+/-)}$ Dia displayed a thin ECM (supplementary material, Figure S4B). As expected, the Dia of Nfix$^{fl/fl}$:α$^{(-/-)}$ mice contained large ECM deposits that increased from 2 to 6 months (supplementary material, Figure S4B). The Dia of ΦNfix$^{(-/-)}$:α$^{(-/-)}$ mice showed zones of

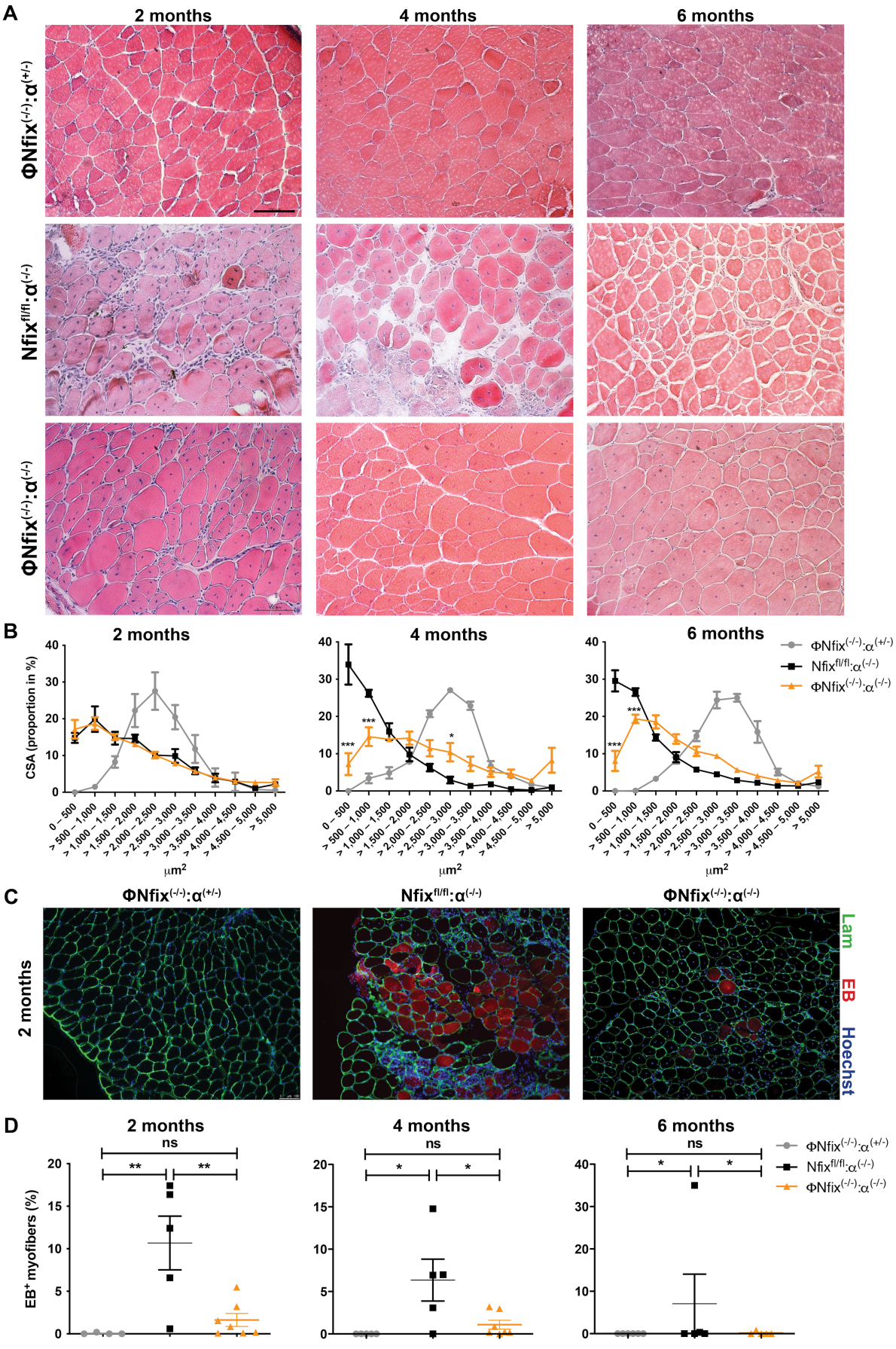

Figure 2 Legend on next page.

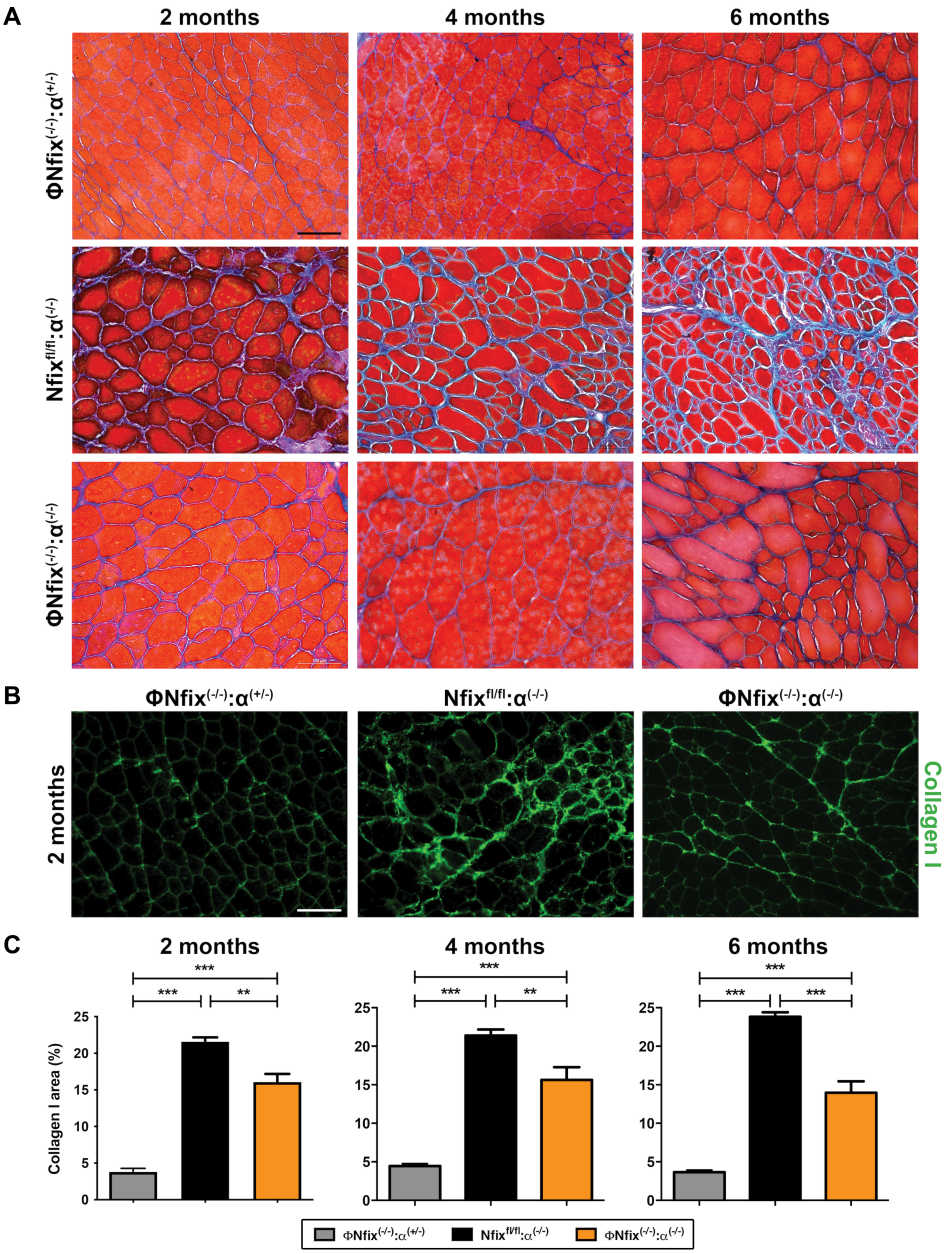

Figure 3. Ablation of Nfix in MPs delays fibrosis. (A) Milligan trichrome staining of ΦNfix$^{(-/-)}$:α$^{(+/-)}$, Nfix$^{fl/fl}$:α$^{(-/-)}$, and ΦNfix$^{(-/-)}$:α$^{(-/-)}$ TA muscles at 2, 4, and 6 months of age. (B) Immunofluorescence for collagen I (green) of ΦNfix$^{(-/-)}$:α$^{(+/-)}$, Nfix$^{fl/fl}$:α$^{(-/-)}$, and ΦNfix$^{(-/-)}$:α$^{(-/-)}$ TA muscles at 2 months of age. (C) Quantification of collagen I^{+} area at 2, 4, and 6 months of age. Statistical significance was determined using a one-way ANOVA test. $^{**}p < 0.01$, $^{***}p < 0.001$. Means ± SEM. $N = 4$–6 mice per group. Scale bar: 100 µm.

ECM that were thinner compared with the Nfix$^{fl/fl}$:α$^{(-/-)}$ mice (supplementary material, Figure S4B). Quantification of the collagen I area showed an increase in both Nfix$^{fl/fl}$:α$^{(-/-)}$ and ΦNfix$^{(-/-)}$:α$^{(-/-)}$ mice Dia compared with the TA (Figure 4B,C versus Figure 3B,C), but the collagen I area in the Dia of ΦNfix$^{(-/-)}$:α$^{(-/-)}$ mice remained reduced compared with the Nfix$^{fl/fl}$:α$^{(-/-)}$ mice at 4 and 6 months (Figure 4B,C). Thus, the ablation of Nfix in MPs protects the Dia from dystrophy.

Figure 2. Ablation of Nfix in MPs protects dystrophic muscle. (A) H&E staining of ΦNfix$^{(-/-)}$:α$^{(+/-)}$, Nfix$^{fl/fl}$:α$^{(-/-)}$, and ΦNfix$^{(-/-)}$:α$^{(-/-)}$ TA muscles at 2, 4, and 6 months of age. (B) Proportion (%) of the cross-sectional area (CSA). (C) Evans blue (EB, red) and immunofluorescence for Lam (green) and Hoechst (blue) of ΦNfix$^{(-/-)}$:α$^{(+/-)}$, Nfix$^{fl/fl}$:α$^{(-/-)}$, and ΦNfix$^{(-/-)}$:α$^{(-/-)}$ TA muscles at 2 months of age. (D) Percentage of EB^{+} myofibers at 2, 4, and 6 months of age. EB was injected 24 h before sacrifice. Statistical significance was determined using a one-way or a two-way ANOVA test.$^{*}p < 0.05$, $^{**}p < 0.01$. ns, not significant. For B, $^{*}p < 0.05$, $^{***}p < 0.001$ Nfix$^{fl/fl}$:α$^{(-/-)}$ versus ΦNfix$^{(-/-)}$:α$^{(-/-)}$. Means ± SEM. $N = 4$–7 mice per group. Scale bar: 100 µm.

Nfix induces a profibrotic phenotype of MPs in dystrophic muscle

Within the muscle, FAPs are the main source of ECM. In MDs, MPs induce the survival of FAPs, thus leading to fibrosis. In the TA of ΦNfix$^{(-/-)}$:α$^{(-/-)}$ mice, we observed a decrease in the number of FAPs (PDGFRα^{+} cells) and MPs (F4/80^{+} cells) compared with Nfix$^{fl/fl}$:α$^{(-/-)}$ mice (Figure 5A). ECM deposits are due to excessive TGFβ1 signaling, whose expression does not reflect its biological availability. TGFβ1 is secreted in a latent form that is cleaved to be active [32]. As previously shown [33,34], we observed no differences in TGFβ1 expression between our two dystrophic models (supplementary material, Figure S5A), but the analysis of its downstream Smad3 signaling pathway showed a decrease of TGFβ1 pathway activation at 2 and 4 months (Figure 5B). This induces a decrease of FN (*fibronectin 1*) expression but has no effect on αSMA (α-smooth muscle actin; *Acta2*) expression (supplementary material, Figure S5A). After acute injury, pro-inflammatory MPs express TNFα, which induces the apoptosis of FAPs, while TGFβ1 secreted by anti-inflammatory MPs rescues them from TNFα-induced apoptosis and stimulates their proliferation. In a dystrophic context, more than 75% of MPs express TGFβ1, inducing the survival of FAPs [28].

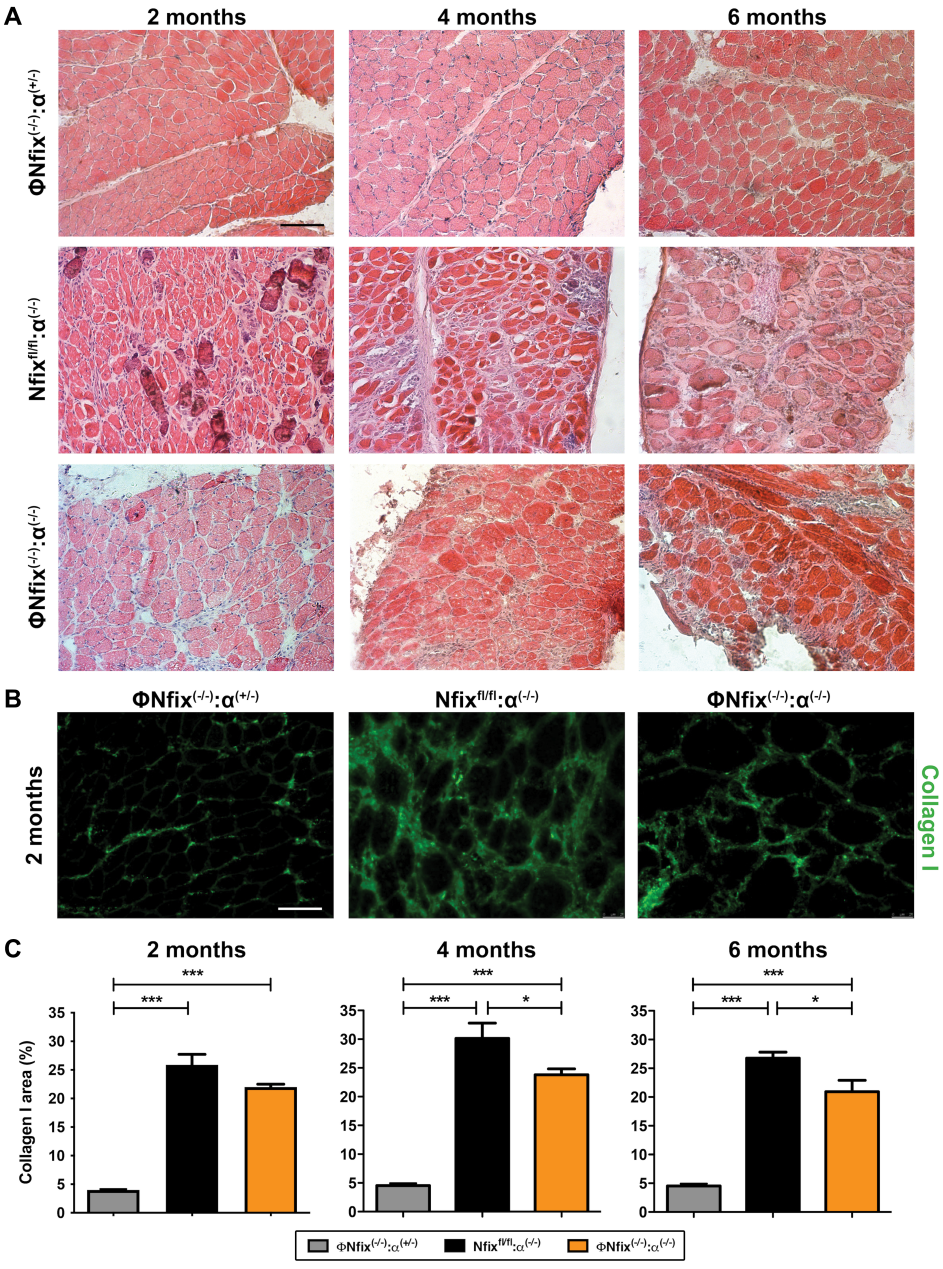

Figure 4. Ablation of Nfix in MPs also preserves the diaphragm (Dia) from fibrosis. (A) H&E staining of ΦNfix$^{(-/-)}$:α$^{(+/-)}$, Nfix$^{fl/fl}$:α$^{(-/-)}$, and ΦNfix$^{(-/-)}$:α$^{(-/-)}$ Dia muscles at 2, 4, and 6 months of age. (B) Immunofluorescence for collagen I (green) of ΦNfix$^{(-/-)}$:α$^{(+/-)}$, Nfix$^{fl/fl}$:α$^{(-/-)}$, and ΦNfix$^{(-/-)}$:α$^{(-/-)}$ Dia muscles at 2 months of age. (C) Quantification of collagen I^{+} area at 2, 4, and 6 months of age. Statistical significance was determined using a one-way ANOVA test. *$p < 0.05$, ***$p < 0.001$. Means ± SEM. $N = 3$–6 mice per group. Scale bar: 100 µm.

Thus, we decided to sort FAPs and MPs from hindlimb muscles of Nfix$^{fl/fl}$:α$^{(-/-)}$ and ΦNfix$^{(-/-)}$:α$^{(-/-)}$ mice (supplementary material, Figure S5B,C). This analysis confirmed the decrease of the numbers of FAPs and MPs within the muscles of ΦNfix$^{(-/-)}$:α$^{(-/-)}$ mice compared with those of Nfix$^{fl/fl}$:α$^{(-/-)}$ mice (supplementary

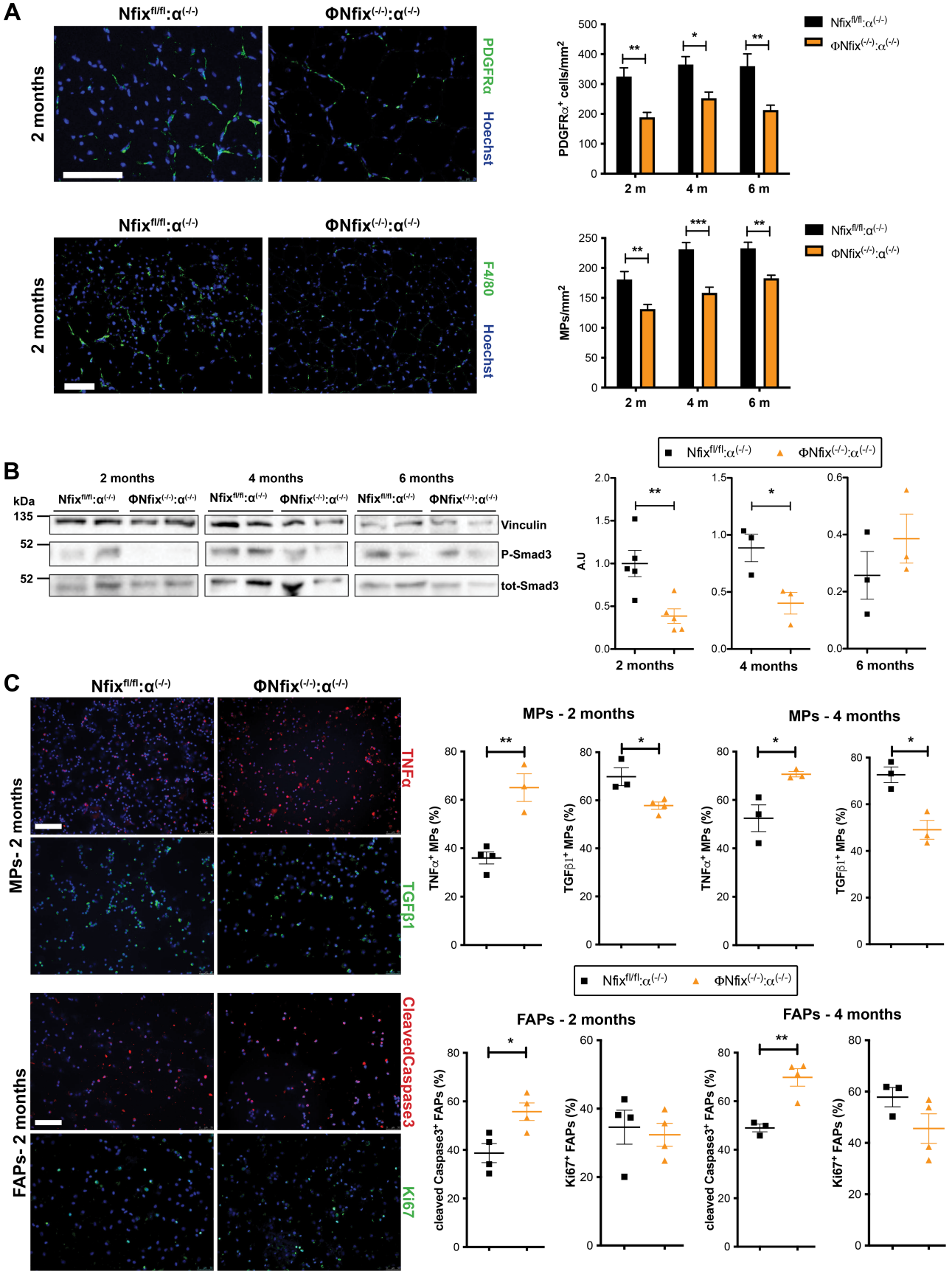

Figure 5 Legend on next page.

material, Figure S5D). Then we quantified the number of MPs positive for TNFα or TGFβ1 and the number of apoptotic or proliferating FAPs (Figure 5C). We observed an increase of $TNF\alpha^{+}$ MPs and a decrease of $TGF\beta1^{+}$ MPs in $\Phi Nfix^{(-/-)}$:$\alpha^{(-/-)}$ mice compared with $Nfix^{fl/fl}$:$\alpha^{(-/-)}$ mice. This modification of cytokine expression did not modify the proliferation of FAPs but induced their apoptosis (Figure 5C). The proportions of $Ly6C^{+}$ and $Ly6C^{-}$ MPs were unchanged between $Nfix^{fl/fl}$:$\alpha^{(-/-)}$ and $\Phi Nfix^{(-/-)}$:$\alpha^{(-/-)}$ mice, meaning that the Ly6C receptor does not define a pro- and anti-inflammatory-like MP population in dystrophic muscle (supplementary material, Figure S5E). To conclude, we observed that Nfix is involved in the profibrotic phenotype of MPs and that its deletion rebalances TNFα–TGFβ1 expression, promoting apoptosis of FAPs.

Pharmacological inhibition of ROCK in dystrophic muscle promotes fibrosis by inducing Nfix in MPs

We previously demonstrated that Nfix is expressed upon RhoA/ROCK-dependent phagocytosis after muscle acute injury [25]; thus, we asked whether this pathway was conserved in a dystrophic context and if the stimulation of Nfix expression by MPs could accelerate fibrosis. Therefore, we treated *Sgca* null mice with Y27632 ROCK inhibitor (hereafter called Y) or its control, 3 times per week for 2 weeks. $\Phi Nfix^{(-/-)}$:$\alpha^{(-/-)}$ mice were also treated to distinguish the effect of ROCK inhibition on MPs with respect to other cell types (supplementary material, Figure S6A). Y treatment increased ECM deposits within the TA of *Sgca* null mice compared with control-treated *Sgca* null mice, while this effect was not observed in Y-treated $\Phi Nfix^{(-/-)}$:$\alpha^{(-/-)}$ mice compared with control-treated $\Phi Nfix^{(-/-)}$:$\alpha^{(-/-)}$ mice (Figure 6A). In *Sgca* null mice, Y injection induced an increase of MPs positive for Nfix (Figure 6B). In control and Y-injected $\Phi Nfix^{(-/-)}$:$\alpha^{(-/-)}$ mice, around 15% of MPs were positive for Nfix (Figure 6B). This result is in line with our study showing that resident MPs are positive for Nfix in uninjured muscle and that around 10% of resident MPs are $Nfix^{+}$ [25]. While Y injection did not modify the number of MPs/mm^2 in each murine model, the number of MPs positive for Nfix increased in *Sgca* null and not in $\Phi Nfix^{(-/-)}$:$\alpha^{(-/-)}$ mice (Figure 6B and supplementary material, Figure S6B). Thus, the increase of $Nfix^{+}$ MPs in treated *Sgca* null mice was due to a modification of the MP phenotype and not to an increase of infiltrated MPs. This phenomenon is not observed in $\Phi Nfix^{(-/-)}$:$\alpha^{(-/-)}$ mice. We previously reported that Nfix overexpression in myofibers exacerbates the dystrophic phenotype and that ROCK inhibition induces Nfix expression in embryonic myoblasts but not in juvenile satellite cells (SCs) [24,35]. Here, we observed that Y treatment in both *Sgca* null mice and $\Phi Nfix^{(-/-)}$:$\alpha^{(-/-)}$ mice had no effect on Nfix expression by SCs but decreased the number of SCs per mm^2 (supplementary material, Figure S6C). On the contrary, we observed an increase in the percentage of $Nfix^{+}$ myofibers, suggesting that ROCK inhibition stimulates Nfix expression by myofibers (supplementary material, Figure S6D). While our previous study on the overexpression of Nfix in myofibers showed a decreased CSA and an increase of the percentage of centronucleated myofibers, ROCK inhibition did not modify these two parameters or the number of myonuclei/myofibers in *Sgca* null mice or $\Phi Nfix^{(-/-)}$:$\alpha^{(-/-)}$ mice versus their respective controls (supplementary material, Figure S6D). We observed an increase of CSA in the TA of $\Phi Nfix^{(-/-)}$:$\alpha^{(-/-)}$ mice compared with *Sgca* null mice and an increase in the percentage of perinucleated myofibers (supplementary material, Figure S6D). Y injection increased collagen I deposits and the number of FAPs in *Sgca* null mice and not in $\Phi Nfix^{(-/-)}$:$\alpha^{(-/-)}$ mice (Figure 6C,D). Although we cannot exclude a role for Nfix in other cell types, such as the same FAPs, we can conclude that the pharmacological inhibition of ROCK promotes fibrosis at least by increasing Nfix expression in MPs.

Discussion

MDs are incurable diseases and although several approaches such as cellular or gene therapies aim to treat MDs, these have been demonstrated to be of low clinical benefit so far [36-38]. Most of these strategies are obviously focused on muscle cells, which are at the origin of the disease; it is now clear that non-muscle cells, and particularly MPs, play a role in MD progression [20,27,39-42]. In this study, we used the $LysM^{CRE}$ mouse model to delete Nfix in MPs, although neutrophils also express LysM. However, in *Sgca* null mice, macrophages are much more prevalent in the dystrophic muscle compared with neutrophils [17], and in our

Figure 5. MPs lacking Nfix rescue FAP apoptosis by reducing TGFβ1 signaling and expressing TNFα. (A) Top panels: immunofluorescence for PDGFRα (green) and Hoechst (blue) of $Nfix^{fl/fl}$:$\alpha^{(-/-)}$ and $\Phi Nfix^{(-/-)}$:$\alpha^{(-/-)}$ TA muscles at 2 months of age, and number of $PDGFR\alpha^{+}$ cells per mm^2. Bottom panels: immunofluorescence for F4/80 (green) and Hoechst (blue) of $Nfix^{fl/fl}$:$\alpha^{(-/-)}$ and $\Phi Nfix^{(-/-)}$:$\alpha^{(-/-)}$ TA muscles at 2 months of age, and number of MPs^{+} per mm^2. (B) Representative immunoblot for P-Smad3 and tot-Smad3 in $Nfix^{fl/fl}$:$\alpha^{(-/-)}$ and $\Phi Nfix^{(-/-)}$:$\alpha^{(-/-)}$ TA muscles at 2 months of age and quantification. Immunoblots were realized on two different membranes or the membrane was stripped, and vinculin was used for normalization (see supplementary material, Figure S7). (C) Immunofluorescence for TNFα (red) or TGFβ1 (green) and Hoechst (blue) on cytospinned sorted MPs (top panels, left) and for cleaved caspase-3 (red) or Ki67 (green) and Hoechst (blue) on cytospinned sorted FAPs (bottom panels, left) and percentage of TNFα- or TGFβ1-positive MPs (top, right) and cleaved caspase-3- or Ki67-positive FAPs (bottom, right) sorted from $Nfix^{fl/fl}$:$\alpha^{(-/-)}$ and $\Phi Nfix^{(-/-)}$:$\alpha^{(-/-)}$ hindlimb muscles at 2 and 4 months of age. Statistical significance was determined using a two-tailed Student's *t*-test or a two-way ANOVA test. $^{*}p < 0.05$, $^{**}p < 0.01$. Means ± SEM. $N = 3$–11 mice per group. Scale bar: 100 µm.

previous study, LysM^{CRE}:Nfix$^{fl/fl}$ mice exhibited a defect of muscle regeneration after the disappearance of neutrophils in the injured muscle [25]. Thus, the effect of Nfix deletion observed in *Sgca* null dystrophic muscle is likely mainly carried by macrophages than by neutrophils. Recently, several studies demonstrated that the

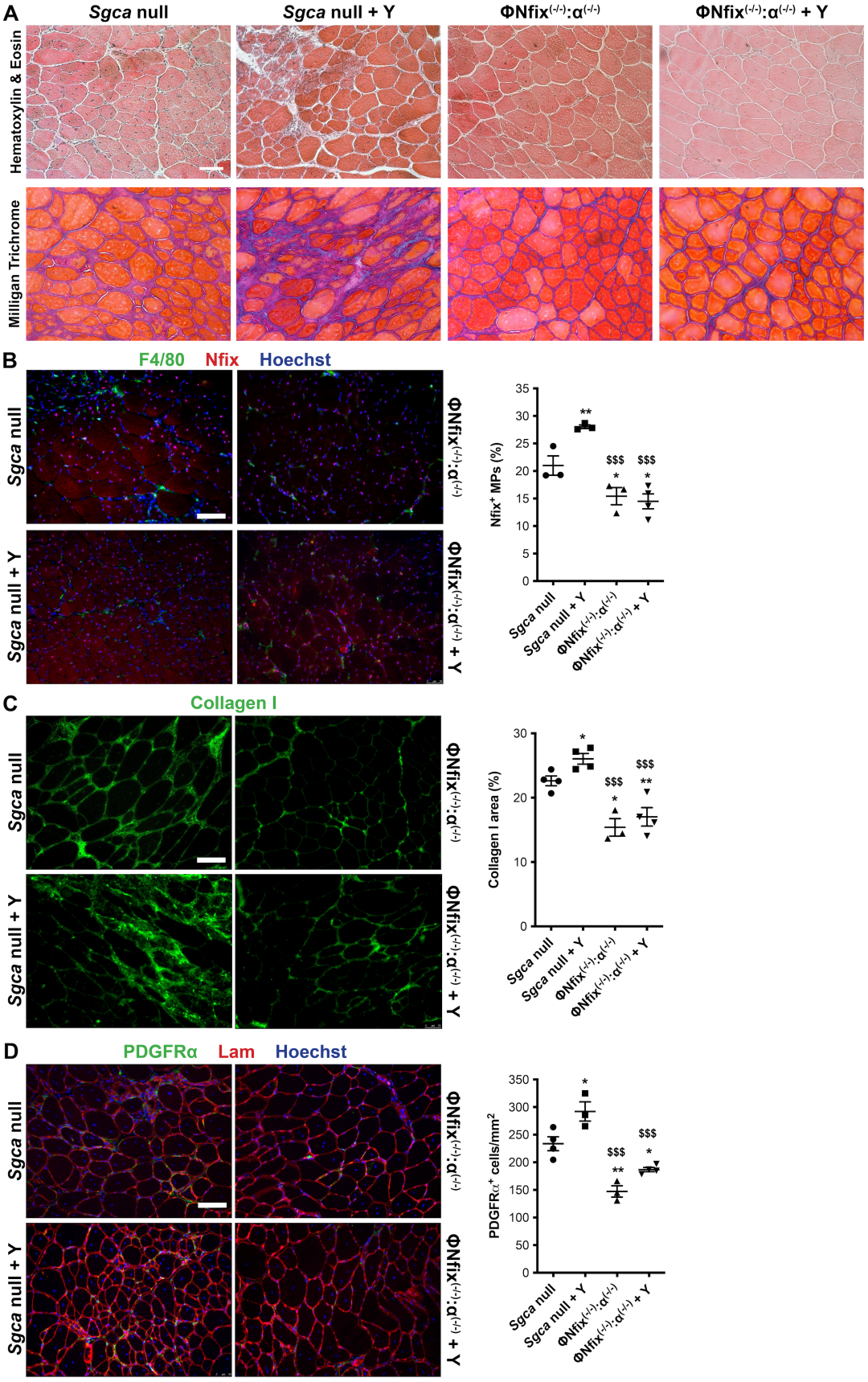

Figure 6 Legend on next page.

expression of foreign Cre recombinase has unanticipated effects on the biology of cells and, as a consequence, on the physiology of tissues [43–45]. These studies used a $CreER^T$ and αMHC-MerCreMer model in which the Cre is active upon tamoxifen injection. Here, we used the $LysM^{CRE}$ (B6.129P2-Lyz2tm1(cre)Ifo/J) mouse, which is not an inducible Cre mouse. While $CreER^T$ and αMHC-MerCreMer induce cell apoptosis, we did not observe any difference in macrophage infiltration after cardiotoxin injection or in the number of macrophages in resting muscle between $LysM^{CRE}$:$Nfix^{fl/fl}$ and $Nfix^{fl/fl}$ mice [25]. More importantly, several studies using the same $LysM^{CRE}$ mouse model observed that the presence of Cre has no effect on macrophage phenotype and function in different tissues [46–49]. Moreover, we previously demonstrated that macrophages infected with lentivirus carrying shNfix display the same impairment of anti-inflammatory phenotype acquisition as $LysM^{CRE}$:$Nfix^{fl/fl}$ macrophages [25]. In addition, we showed that activation of the ROCK pathway in Sgca *null* mice induces Nfix expression in the macrophage population which in turn leads to fibrosis (Figure 6), thus excluding a possible effect due to $LysM^{CRE}$.

Here, we demonstrated that expression of the transcription factor Nfix induces profibrotic features in MPs in a chronic muscle injury context. MPs in which Nfix is deleted secrete more TNFα and less TGFβ1, pushing FAPs towards apoptosis. Pharmacological treatment of *Sgca* null mice with the ROCK inhibitor shapes MPs towards Nfix expression, inducing the persistence of FAPs and exacerbating fibrosis. Genetic deletion of Nfix in MPs rescues dystrophic muscle by decreasing myofiber death, and some studies have already demonstrated the protective effect of MPs on extensive tissue damage or cellular death [50-52]. Thus, in our $\Phi Nfix^{(-/-)}$:$\alpha^{(-/-)}$ murine model, myofibers probably enter late in degeneration/regeneration cycles, explaining the decrease of regenerative centronucleated myofibers at 2 months compared with $Nfix^{fl/fl}$:$\alpha^{(-/-)}$ mice. This protective effect also acts on the caliber of myofibers: while an increase of the percentage of small myofibers was observed in $Nfix^{fl/fl}$:$\alpha^{(-/-)}$ mice in time, the distribution of myofiber size was unchanged from 2 to 6 months in $\Phi Nfix^{(-/-)}$:$\alpha^{(-/-)}$ mice. The mechanisms linking MPs to fibrosis are beginning to be better known now. It has been shown that MPs are the main source of TGFβ1 that promotes FAP survival and collagen I expression but also reprograms endothelial cells and SCs toward a fibrotic phenotype [17,28,53,54]. Here, we observed that Nfix is a profibrotic factor in MPs, since its absence rebalances cytokines secretion toward more TNFα and less TGFβ1. Moreover, since asynchronous muscle regeneration has been associated with inflammation and fibrotic signatures [55], our study shows that Nfix deletion in MPs rescues MDs from fibrosis directly by inducing FAP apoptosis and indirectly by protecting myofibers from injury. Importantly, the histological improvement of dystrophic muscle correlates with an increase of grasp force.

We previously demonstrated that the RhoA/ROCK-dependent phagocytosis pathway induces Nfix expression during skeletal muscle regeneration upon acute injury [25]. Here, we observed that pushing Nfix expression in MPs by treating *Sgca* null mice with a ROCK inhibitor accelerates the establishment of fibrosis. Recently, two studies demonstrated that RhoA is important for niche retention and maintenance of the myogenic capacity of SCs. Indeed, inhibition of ROCK accelerates muscle regeneration after acute injury [56,57]. In overload conditions, RhoA loss in myofibers impairs hypertrophy by decreasing the number of myonuclei/myofibers, due to less fusion of SCs with myofibers [58]. In our two murine models, ROCK inhibition did not modify the number of SCs expressing Nfix, but we observed a decrease in the number of SCs per mm^2 that is consistent with previous studies [56,57]. In contrast, we observed an increase of $Nfix^+$ myofibers, suggesting that the ROCK/Nfix pathway is conserved in muscle fibers. While overexpression of Nfix in myofibers exacerbates dystrophy by decreasing the caliber of myofibers and increasing the percentage of centronucleated myofibers [24], the increase of $Nfix^+$ myofibers in both Y-injected *Sgca* null mice and $\Phi Nfix^{(-/-)}$:$\alpha^{(-/-)}$ mice has no effect on these two parameters. Similarly, we did not observe a modification of the number of myonuclei within myofibers. Thus, the effect of ROCK inhibition on the number of SCs and the percentage of Nfix-expressing myofibers does not correlate with a modification of muscle features. This could be explained by the fact that chronic muscle injury is a different situation compared with overload-induced hypertrophy or muscle regeneration after acute injury. We previously observed that the exacerbation of the dystrophic phenotype in dystrophic mice overexpressing Nfix in myofibers correlates with an increase of Nfix levels in muscle cells [24]; here, it is also possible that our treatment was not sufficient to reach a level of Nfix that might be deleterious for dystrophic muscle.

Dystrophin/utrophin double knockout mice treated with a ROCK inhibitor demonstrate a reduction of heterotopic ossification in skeletal muscle and heart [59,60]. In contrast to the *mdx* and *Sgca* null mice, the dystrophin/utrophin double knockout mouse model has a more

Figure 6. Pharmacological ROCK inhibition induces fibrosis through increase of $Nfix^+$ MPs. (A) H&E and Milligan trichrome staining of *Sgca* null and $\Phi Nfix^{(-/-)}$:$\alpha^{(-/-)}$ TA muscles injected i.p. with saline solution or Y27632 (hereafter called Y). (B) Immunostaining for Nfix (red), F4/80 (green), and Hoechst (blue) of *Sgca* null and $\Phi Nfix^{(-/-)}$:$\alpha^{(-/-)}$ TA muscles injected i.p. with saline solution or Y, and percentage of double $Nfix^+$/$F4/80^+$ cells. (C) Immunofluorescence for collagen I (green) of *Sgca* null and $\Phi Nfix^{(-/-)}$:$\alpha^{(-/-)}$ TA muscles injected i.p. with saline solution or Y, and percentage of collagen I^+ area. (D) Immunofluorescence for Lam (red), PDGFRα (green), and Hoechst (blue) of *Sgca* null and $\Phi Nfix^{(-/-)}$:$\alpha^{(-/-)}$ TA muscles injected i.p. with saline solution or Y, and number of $PDGFR\alpha^+$ cells per mm^2. Statistical significance was determined using a two-tailed Student's *t*-test or a one-way ANOVA test. * versus *Sgca* null: $^*p < 0.05$, $^{**}p < 0.01$. $^\$$ versus *Sgca* null + Y: $^{\$\$\$}p < 0.001$. Means ± SEM. $N = 3$ or 4 mice per group. Scale bar: 50 µm.

severe phenotype which is closer to that of DMD patients [61-63]. They develop calcification within skeletal muscle [64], whereas in *Sgca* null mice, calcification represents less than 1% of the area of several muscles [29]. Indeed, the formation of heterotopic ossification seems to be linked to the total absence of dystrophin expression [65], but the dystrophin, even if reduced, is still present in dystrophic muscles of *Sgca* null mice [26]. This could explain differences observed upon ROCK inhibition treatment between these two murine models. Nevertheless, we observed that the increase of ECM deposits and the number of FAPs occur only in Y-treated *Sgca* null mice and not in $\Phi Nfix^{(-/-)}$:$\alpha^{(-/-)}$ mice, correlating with the number of MPs expressing Nfix without modifying the total number of MPs present in the muscle. This demonstrates that pushing the MP phenotype through Nfix expression is sufficient to promote fibrosis.

Considering therapy, to delay the progression of MD it seems preferable to modulate the MP phenotype rather than reduce the abundance of MPs within the muscle. Indeed, the decrease of MP infiltration through to the deletion of CCR2 in *mdx* has beneficial effects in the short term (12 weeks) which are lost at 6 months [11,66]. Here, we observed an improvement of dystrophic histopathology that is conserved until 6 months, and an improvement of grasp force at early stages. The deletion of Nfix in myogenic cells leads to benefits in terms of oxidative phenotype and improvement of muscle function during forced running [24], while deletion of Nfix in MPs plays more on the protection of muscle fibers, inhibition of fibrosis, and increasing grasp strength. Importantly, we observed some MPs positive for Nfix in the muscles of $\Phi Nfix^{(-/-)}$:$\alpha^{(-/-)}$ mice; thus, complete depletion of $Nfix^{+}$ macrophages could induce a major rescue of muscular dystrophy. Therefore, targeting Nfix in both myogenic cells and MPs could be useful to preserve musculature in MD patients. Prospectively, transcriptome analysis of macrophages within $\Phi Nfix^{(-/-)}$:$\alpha^{(-/-)}$ dystrophic muscle would be interesting to better understand the effect of Nfix deletion on macrophage phenotype and function.

Several techniques using nanoparticles, liposomes or nanogels to encapsulate drugs and use MPs as drug carriers, but also as drug targets, are now under development [67-69]. Moreover, MPs efficiently take up large amounts of phosphorodiamidate morpholino oligomers to deliver them to myoblasts in dystrophic lesions [70]. Thus, we can speculate that upon Nfix inhibition, MPs would change phenotype and protect dystrophic muscle, even by delivering drugs to myogenic cells. Of course, the question of the muscle specificity of drugs that selectively inhibit Nfix in both cell types has to be addressed, but it could be a promising way to delay both muscle loss and fibrosis progression in MDs.

Acknowledgements

We thank R Gronostajski for the kind exchange of information and animal models. We are also grateful to B Chazaud and R Mounier for helpful discussions and the exchange of animal models. We thank G Caretti and L Nevi for their help with the grasp test and kindly lending the dynamometer. This research was funded by Association Française contre les Myopathies AFM-Telethon (grant number 20002) and the European Community, ERCStG2011 (RegeneratioNfix 280611). Open Access Funding provided by Universita degli Studi di Milano within the CRUI-CARE Agreement. [Correction added on May 19, 2022, after first online publication: CRUI funding statement has been added.]

Author contributions statement

MS designed and performed experiments, analyzed data, interpreted results, and wrote the paper. GT and CB performed experiments and analyzed data. GA and GMu performed experiments during the review process. GMe supervised the work and wrote the paper. All the authors read and approved the final paper.

References

1. Ervasti JM, Campbell KP. Dystrophin and the membrane skeleton. *Curr Opin Cell Biol* 1993; **5:** 82–87.
2. Barton ER. Impact of sarcoglycan complex on mechanical signal transduction in murine skeletal muscle. *Am J Physiol Cell Physiol* 2006; **290:** C411–C419.
3. Rando TA. The dystrophin–glycoprotein complex, cellular signaling, and the regulation of cell survival in the muscular dystrophies. *Muscle Nerve* 2001; **24:** 1575–1594.
4. Emery AEH. The muscular dystrophies. *Lancet* 2002; **359:** 687–695.
5. Emery AEH. Fortnightly review: the muscular dystrophies. *BMJ* 1998; **317:** 991–995.
6. Griggs RC, Moxley RT 3rd, Mendell JR, *et al*. Prednisone in Duchenne dystrophy. A randomized, controlled trial defining the time course and dose response. Clinical Investigation of Duchenne Dystrophy Group. *Arch Neurol* 1991; **48:** 383–388.
7. Hoffman EP, Monaco AP, Feener CC, *et al*. Conservation of the Duchenne muscular dystrophy gene in mice and humans. *Science* 1987; **238:** 347–350.
8. Joseph S, Wang C, Bushby K, *et al*. Fractures and linear growth in a nationwide cohort of boys with Duchenne muscular dystrophy with and without glucocorticoid treatment: results from the UK Northstar Database. *JAMA Neurol* 2019; **76:** 701–709.
9. Bylo M, Farewell R, Coppenrath VA, *et al*. A review of deflazacort for patients with Duchenne muscular dystrophy. *Ann Pharmacother* 2020; **54:** 788–794.
10. Giordano C, Mojumdar K, Liang F, *et al*. Toll-like receptor 4 ablation in mdx mice reveals innate immunity as a therapeutic target in Duchenne muscular dystrophy. *Hum Mol Genet* 2015; **24:** 2147–2162.
11. Mojumdar K, Liang F, Giordano C, *et al*. Inflammatory monocytes promote progression of Duchenne muscular dystrophy and can be therapeutically targeted via CCR2. *EMBO Mol Med* 2014; **6:** 1476–1492.
12. Wehling M, Spencer MJ, Tidball JG. A nitric oxide synthase transgene ameliorates muscular dystrophy in mdx mice. *J Cell Biol* 2001; **155:** 123–131.
13. Madaro L, Torcinaro A, De Bardi M, *et al*. Macrophages fine tune satellite cell fate in dystrophic skeletal muscle of mdx mice. *PLoS Genet* 2019; **15:** e1008408.

14. Zhou L, Porter JD, Cheng G, *et al*. Temporal and spatial mRNA expression patterns of TGF-beta1, 2, 3 and TbetaRI, II, III in skeletal muscles of mdx mice. *Neuromuscul Disord* 2006; **16:** 32–38.
15. Gosselin LE, Williams JE, Deering M, *et al*. Localization and early time course of TGF-beta 1 mRNA expression in dystrophic muscle. *Muscle Nerve* 2004; **30:** 645–653.
16. Ismaeel A, Kim JS, Kirk JS, *et al*. Role of transforming growth factor-beta in skeletal muscle fibrosis: a review. *Int J Mol Sci* 2019; **20:** 2446.
17. Juban G, Saclier M, Yacoub-Youssef H, *et al*. AMPK activation regulates LTBP4-dependent TGF-β1 secretion by pro-inflammatory macrophages and controls fibrosis in Duchenne muscular dystrophy. *Cell Rep* 2018; **25:** 2163–2176.e6.
18. Acharyya S, Villalta SA, Bakkar N, *et al*. Interplay of IKK/NF-kappaB signaling in macrophages and myofibers promotes muscle degeneration in Duchenne muscular dystrophy. *J Clin Invest* 2007; **117:** 889–901.
19. Hamoudi D, Marcadet L, Piette Boulanger A, *et al*. An anti-RANKL treatment reduces muscle inflammation and dysfunction and strengthens bone in dystrophic mice. *Hum Mol Genet* 2019; **28:** 3101–3112.
20. Theret M, Saclier M, Messina G, *et al*. Macrophages in skeletal muscle dystrophies, an entangled partner. *J Neuromuscul Dis* 2022; **9:** 1–23.
21. Gronostajski RM. Roles of the NFI/CTF gene family in transcription and development. *Gene* 2000; **249:** 31–45.
22. Messina G, Biressi S, Monteverde S, *et al*. Nfix regulates fetal-specific transcription in developing skeletal muscle. *Cell* 2010; **140:** 554–566.
23. Rossi G, Antonini S, Bonfanti C, *et al*. Nfix regulates temporal progression of muscle regeneration through modulation of myostatin expression. *Cell Rep* 2016; **14:** 2238–2249.
24. Rossi G, Bonfanti C, Antonini S, *et al*. Silencing Nfix rescues muscular dystrophy by delaying muscle regeneration. *Nat Commun* 2017; **8:** 1055.
25. Saclier M, Lapi M, Bonfanti C, *et al*. The transcription factor Nfix requires RhoA-ROCK1 dependent phagocytosis to mediate macrophage skewing during skeletal muscle regeneration. *Cells* 2020; **9:** 708.
26. Duclos F, Straub V, Moore SA, *et al*. Progressive muscular dystrophy in alpha-sarcoglycan-deficient mice. *J Cell Biol* 1998; **142:** 1461–1471.
27. Muñoz-Cánoves P, Serrano AL. Macrophages decide between regeneration and fibrosis in muscle. *Trends Endocrinol Metab* 2015; **26:** 449–450.
28. Lemos DR, Babaeijandaghi F, Low M, *et al*. Nilotinib reduces muscle fibrosis in chronic muscle injury by promoting TNF-mediated apoptosis of fibro/adipogenic progenitors. *Nat Med* 2015; **21:** 786–794.
29. Verhaart IEC, Putker K, van de Vijver D, *et al*. Cross-sectional study into age-related pathology of mouse models for limb girdle muscular dystrophy types 2D and 2F. *PLoS One* 2019; **14:** e0220665.
30. Pastoret C, Sebille A. *mdx* mice show progressive weakness and muscle deterioration with age. *J Neurol Sci* 1995; **129:** 97–105.
31. Pasteuning-Vuhman S, Putker K, Tanganyika-de Winter CL, *et al*. Natural disease history of mouse models for limb girdle muscular dystrophy types 2D and 2F. *PLoS One* 2017; **12:** e0182704.
32. Travis MA, Sheppard D. TGF-β activation and function in immunity. *Annu Rev Immunol* 2014; **32:** 51–82.
33. Onofre-Oliveira PCG, Santos ALF, Martins PM, *et al*. Differential expression of genes involved in the degeneration and regeneration pathways in mouse models for muscular dystrophies. *Neuromolecular Med* 2012; **14:** 74–83.
34. Andreetta F, Bernasconi P, Baggi F, *et al*. Immunomodulation of TGF-beta 1 in mdx mouse inhibits connective tissue proliferation in diaphragm but increases inflammatory response: implications for antifibrotic therapy. *J Neuroimmunol* 2006; **175:** 77–86.
35. Taglietti V, Angelini G, Mura G, *et al*. RhoA and ERK signalling regulate the expression of the transcription factor Nfix in myogenic cells. *Development* 2018; **145:** dev163956.
36. Biressi S, Filareto A, Rando TA. Stem cell therapy for muscular dystrophies. *J Clin Invest* 2020; **130:** 5652–5664.
37. Himič V, Davies KE. Evaluating the potential of novel genetic approaches for the treatment of Duchenne muscular dystrophy. *Eur J Hum Genet* 2021; **29:** 1369–1376.
38. Roy B, Griggs R. Advances in treatments in muscular dystrophies and motor neuron disorders. *Neurol Clin* 2021; **39:** 87–112.
39. Cappellari O, Mantuano P, De Luca A. "The Social Network" and muscular dystrophies: the lesson learnt about the niche environment as a target for therapeutic strategies. *Cells* 2020; **9:** 1659.
40. Biferali B, Proietti D, Mozzetta C, *et al*. Fibro–adipogenic progenitors cross-talk in skeletal muscle: the social network. *Front Physiol* 2019; **10:** 1074.
41. Dort J, Fabre P, Molina T, *et al*. Macrophages are key regulators of stem cells during skeletal muscle regeneration and diseases. *Stem Cells Int* 2019; **2019:** 4761427.
42. Villalta SA, Rosenberg AS, Bluestone JA. The immune system in Duchenne muscular dystrophy: friend or foe. *Rare Dis* 2015; **3:** e1010966.
43. Pépin G, Ferrand J, Höning K, *et al*. Cre-dependent DNA recombination activates a STING-dependent innate immune response. *Nucleic Acids Res* 2016; **44:** 5356–5364.
44. Lexow J, Poggioli T, Sarathchandra P, *et al*. Cardiac fibrosis in mice expressing an inducible myocardial-specific Cre driver. *Dis Model Mech* 2013; **6:** 1470–1476.
45. Bersell K, Choudhury S, Mollova M, *et al*. Moderate and high amounts of tamoxifen in *αmHC-MerCreMer* mice induce a DNA damage response, leading to heart failure and death. *Dis Model Mech* 2013; **6:** 1459–1469.
46. Gondin J, Théret M, Duhamel G, *et al*. Myeloid HIFs are dispensable for resolution of inflammation during skeletal muscle regeneration. *J Immunol* 2015; **194:** 3389–3399.
47. Zlatanova I, Pinto C, Bonnin P, *et al*. Iron regulator hepcidin impairs macrophage-dependent cardiac repair after injury. *Circulation* 2019; **139:** 1530–1547.
48. Gao R, Peng X, Perry C, *et al*. Macrophage-derived netrin-1 drives adrenergic nerve-associated lung fibrosis. *J Clin Invest* 2021; **131:** e136542.
49. Unrau L, Endig J, Goltz D, *et al*. Smad7 deficiency in myeloid cells does not affect liver injury, inflammation or fibrosis after chronic CCl_4 exposure in mice. *Int J Mol Sci* 2021; **22:** 11575.
50. Sonnet C, Lafuste P, Arnold L, *et al*. Human macrophages rescue myoblasts and myotubes from apoptosis through a set of adhesion molecular systems. *J Cell Sci* 2006; **119:** 2497–2507.
51. Uderhardt S, Martins AJ, Tsang JS, *et al*. Resident macrophages cloak tissue microlesions to prevent neutrophil-driven inflammatory damage. *Cell* 2019; **177:** 541–555.e17.
52. Liu Y, Verma VK, Malhi H, *et al*. Lipopolysaccharide downregulates macrophage-derived IL-22 to modulate alcohol-induced hepatocyte cell death. *Am J Physiol Cell Physiol* 2017; **313:** C305–C313.
53. Pessina P, Kharraz Y, Jardí M, *et al*. Fibrogenic cell plasticity blunts tissue regeneration and aggravates muscular dystrophy. *Stem Cell Reports* 2015; **4:** 1046–1060.
54. Vidal B, Serrano AL, Tjwa M, *et al*. Fibrinogen drives dystrophic muscle fibrosis via a TGFbeta/alternative macrophage activation pathway. *Genes Dev* 2008; **22:** 1747–1752.
55. Dadgar S, Wang Z, Johnston H, *et al*. Asynchronous remodeling is a driver of failed regeneration in Duchenne muscular dystrophy. *J Cell Biol* 2014; **207:** 139–158.
56. You JS, Singh N, Reyes-Ordonez A, *et al*. ARHGEF3 regulates skeletal muscle regeneration and strength through autophagy. *Cell Rep* 2021; **34:** 108594.

57. Eliazer S, Muncie JM, Christensen J, *et al*. Wnt4 from the niche controls the mechano-properties and quiescent state of muscle stem cells. *Cell Stem Cell* 2019; **25:** 654–665.e4.
58. Noviello C, Kobon K, Delivry L, *et al*. RhoA within myofibers controls satellite cell microenvironment to allow hypertrophic growth. *iScience* 2021; **25:** 103616.
59. Mu X, Usas A, Tang Y, *et al*. RhoA mediates defective stem cell function and heterotopic ossification in dystrophic muscle of mice. *FASEB J* 2013; **27:** 3619–3631.
60. Mu X, Lin CY, Hambright WS, *et al*. Aberrant RhoA activation in macrophages increases senescence-associated secretory phenotypes and ectopic calcification in muscular dystrophic mice. *Aging (Albany NY)* 2020; **12:** 24853–24871.
61. Janssen PML, Hiranandani N, Mays TA, *et al*. Utrophin deficiency worsens cardiac contractile dysfunction present in dystrophin-deficient *mdx* mice. *Am J Physiol Heart Circ Physiol* 2005; **289:** H2373–H2378.
62. Deconinck AE, Rafael JA, Skinner JA, *et al*. Utrophin–dystrophin-deficient mice as a model for Duchenne muscular dystrophy. *Cell* 1997; **90:** 717–727.
63. Grady RM, Teng H, Nichol MC, *et al*. Skeletal and cardiac myopathies in mice lacking utrophin and dystrophin: a model for Duchenne muscular dystrophy. *Cell* 1997; **90:** 729–738.
64. Isaac C, Wright A, Usas A, *et al*. Dystrophin and utrophin "double knockout" dystrophic mice exhibit a spectrum of degenerative musculoskeletal abnormalities. *J Orthop Res* 2013; **31:** 343–349.
65. Young CNJ, Gosselin MRF, Rumney R, *et al*. Total absence of dystrophin expression exacerbates ectopic myofiber calcification and fibrosis and alters macrophage infiltration patterns. *Am J Pathol* 2020; **190:** 190–205.
66. Zhao W, Wang X, Ransohoff RM, *et al*. CCR2 deficiency does not provide sustained improvement of muscular dystrophy in *mdx*^{5cv} mice. *FASEB J* 2017; **31:** 35–46.
67. He W, Kapate N, Shields CW 4th, *et al*. Drug delivery to macrophages: a review of targeting drugs and drug carriers to macrophages for inflammatory diseases. *Adv Drug Deliv Rev* 2020; **165–166:** 15–40.
68. Pei Y, Yeo Y. Drug delivery to macrophages: challenges and opportunities. *J Control Release* 2016; **240:** 202–211.
69. Xia Y, Rao L, Yao H, *et al*. Engineering macrophages for cancer immunotherapy and drug delivery. *Adv Mater* 2020; **32:** e2002054.
70. Novak JS, Hogarth MW, Boehler JF, *et al*. Myoblasts and macrophages are required for therapeutic morpholino antisense oligonucleotide delivery to dystrophic muscle. *Nat Commun* 2017; **8:** 941.

SUPPLEMENTARY MATERIAL ONLINE

Supplementary figure legends

Figure S1. The number of Nfix$^+$ MPs per mm^2 increases with age in *Sgca* null and *mdx* mice

Figure S2. Whole TA muscle histology

Figure S3. Ablation of Nfix in MPs protects dystrophic muscle and improves grasp force

Figure S4. Whole diaphragm (Dia) muscle histology

Figure S5. TGFβ1 expression, gating strategy, and number of MPs and FAPs

Figure S6. Pharmacological ROCK1 inhibition strategy, number of MPs, and Nfix$^+$ SCs

Figure S7. Uncropped immunoblots used to prepare Figure 5